NORGES TEKNISK-NATURVITENSKAPELIGE UNIVERSITET

Error estimates in inverse design of photonic crystals

by

Larisa Beilina, Marte P. Hatlo, Harald E. Krogstad

PREPRINT
NUMERICS NO. 8/2007

NORWEGIAN UNIVERSITY OF SCIENCE AND TECHNOLOGY
TRONDHEIM, NORWAY

This report has URL
http://www.math.ntnu.no/preprint/numerics/2007/N8-2007.pdf
Address: Department of Mathematical Sciences, Norwegian University of Science and Technology, N-7491 Trondheim, Norway.

Error estimates in inverse design of photonic crystals

Larisa Beilina, Marte P. Hatlo, Harald E. Krogstad

September 14, 2007

We present an a posteriori error estimate together with an adaptive finite element method for an inverse design problem applied to reconstruction of the structure of a photonic crystal.

The inverse problem is formulated as an optimal control problem, where we solve the equations of optimality expressing stationarity of an associated Lagrangian. We present an a posteriori error estimate for the error in the Lagrangian which couples residuals of the computed solution to weights of the reconstruction. We show also that weights can be obtained by solving an associated linearized problem for the Hessian of the Lagrangian and thus the value of the error in the reconstructed parameter can be obtained. The performance of the adaptive finite element method and the usefulness of the a posteriori error estimator are illustrated in numerical examples on reconstruction of the structure of a two-dimensional photonic crystal.

Keywords: transient wave equation, inverse scattering, adaptive finite element methods, a posteriori error estimation, hybrid finite element/difference method, photonic crystals.

1 Introduction

Photonic crystals are space-periodic structures of dielectric material used for a variety of electromagnetic applications extending from radio waves to optical wave lengths. In particular, for the last couples of decades, photonic crystals have attracted great interest for their ability to control the propagation of light [15, 21].

Up to some years ago, the design of a photonic crystal was done by forward simulations combined with optimization or intuition. Recent developments in the field have, however, replaced intuitive engineering and raised interesting mathematical problems in the area [20], e.g. linked to numerical simulations for achieving a certain photonic bandgap [1, 12], as well as design and optimization of crystals for other purposes (see [17] for an overview). The bandgap structures optimization and the optimization of waveguide structures are the two main design classes related to photonic crystals. The first class uses level set methods to shape the interface between two materials [10].

In this paper we concentrate on the second design class and seek the structure of a finite photonic crystal by applying a new mesh-adaptive finite element/difference method to an associated inverse problem. The inverse problem consists of reconstructing the unknown material variables, that is, the dielectric permittivity, $\epsilon(x)$, and magnetic permeability,

$\mu(x)$, from measured wave scattering data on parts of the surface of the crystal, given the wave input on other parts. By solving the wave equation with the same input, the material variables are in principle obtained by fitting the computed to the measured data. The problem is formulated as finding a stationary point of a Lagrangian, involving the forward wave equation (the state equation), the backward wave equation (the adjoint equation), and an equation expressing that the gradient with respect to the parameters vanishes. The optimum is found in an iterative process solving for each step the forward and backward wave equations and updating the material coefficients.

We present a new mesh-adaptive method for the inverse problem, developed in [5], that is based on a specially constructed "goal-oriented" a posteriori error estimate which couples residuals of the computed solution to weights in the reconstruction reflecting the sensitivity of the reconstruction obtained by solving an associated linearized problem for the Hessian of the Lagrangian. The derivation follows the main approach to adaptive error control in computational differential equations presented in [14, 3] and references therein.

Finally, numerical experiments on the reconstruction of the structure of a two-dimensional photonic crystal show the possibilities in computational inverse scattering using the adaptive error control.

2 Mathematical model

We will restrict ourselves to the propagation of light in a mixed dielectric medium in a bounded domain $\Omega \subset \mathbb{R}^d,\ d = 2, 3$ with boundary Γ, governed by Maxwell's equations:

$$\begin{aligned}
\frac{\partial D}{\partial t} - \nabla \times H &= -J, && \text{in } \Omega \times (0, T),\\
\frac{\partial B}{\partial t} + \nabla \times E &= 0, && \text{in } \Omega \times (0, T),\\
\nabla \cdot D &= \rho, && \text{in } \Omega \times (0, T),\\
\nabla \cdot B &= 0, && \text{in } \Omega \times (0, T).
\end{aligned} \tag{2.1}$$

Here $E(x, t)$ and $H(x, t)$ are the electric and magnetic fields, whereas $D(x, t)$ and $B(x, t)$ are the electric and magnetic inductions, respectively. We assume that the dielectric permittivity, $\epsilon(x)$, and magnetic permeability, $\mu(x)$, are scalars, so that $D = \epsilon E$ and $B = \mu H$. The material variables as well as the current density, J, and charge density, ρ, are assumed to be piecewise smooth.

By eliminating B and D from (2.1) we obtain two independent second order systems of partial differential equations

$$\begin{aligned}
\epsilon \frac{\partial^2 E}{\partial t^2} + \nabla \times (\mu^{-1} \nabla \times E) &= -\frac{\partial J}{\partial t},\\
\mu \frac{\partial^2 H}{\partial t^2} + \nabla \times (\epsilon^{-1} \nabla \times H) &= \nabla \times (\epsilon^{-1} J),
\end{aligned} \tag{2.2}$$

which may be solved imposing appropriate initial and boundary conditions.

For simplicity, we restrict ourselves to formulation of the problem in terms of $E(x, t)$ and assume that $J = 0$ and $\rho = 0$. Taking into account the vector identity $\nabla \times \nabla \times V = \nabla(\nabla \cdot V) - \triangle V$, we then obtain

$$\epsilon \frac{\partial^2 E}{\partial t^2} - \nabla \cdot (\frac{1}{\mu} \nabla E) = 0, \quad \text{in } \Omega \times (0, T). \tag{2.3}$$

A similar system of equations is valid for H. Thus, the electric and magnetic fields in isotropic medium satisfy wave equations with a wave speed $c(x) = 1/\sqrt{\epsilon(x)\mu(x)}$.

We consider the equation (2.3) in the domain Ω representing the photonic crystal. Let $\Gamma_1 \subset \Gamma$ and $\Gamma_2 = \Gamma \setminus \Gamma_1$. Assume that an impulse v_1 is initialized at the boundary Γ_1 and propagated during time $(0, t_1]$ into Ω.

The forward problem consists of solving (2.3) with the following initial and boundary conditions:

$$\begin{aligned} &E(\cdot, 0) = 0, \ \frac{\partial E}{\partial t}(\cdot, 0) = 0, \ \text{in } \Omega, \\ &\partial_n E\big|_{\Gamma_1} = v_1, \ \text{on } \Gamma_1 \times (0, t_1], \\ &\partial_n E\big|_{\Gamma_1} = 0, \ \text{on } \Gamma_1 \times (t_1, T), \\ &\partial_n E\big|_{\Gamma_2} = 0, \ \text{on } \Gamma_2 \times (0, T). \end{aligned} \tag{2.4}$$

Our goal is to solve the inverse problem for (2.3) and (2.4), or to find the material parameters $\epsilon(x)$ and $\mu(x)$ from knowledge of data at a finite set of observation points on Γ. The data are generated in experiments where impulses are emitted from Γ_1, backscattered by material inhomogeneities, and recorded again on parts of the boundary Γ.

In real applications the data are generated by emitting waves on the surface of the investigated object and are then recorded on parts of the surface of the object. In this paper, data are generated by computing the forward problem (2.3)-(2.4) with given values of the parameters, and the corresponding solution was recorded at parts of the boundary. The coefficients are then "forgotten" and the goal is to reconstruct the coefficients from computed boundary data.

3 A hybrid finite element/difference method

To solve equation (2.3)-(2.4) we use a hybrid FEM/FDM method developed in [9]. The method is obtained by using continuous space-time piecewise linear finite elements on a partially structured mesh in space. The computational space domain Ω is decomposed into a finite element domain Ω_{FEM} with an unstructured mesh and a finite difference domain Ω_{FDM} with a structured mesh, with typically Ω_{FEM} covering only a small part of the Ω. In Ω_{FDM} we use quadrilateral elements in $\mathbf{R}^2$ and hexahedra in $\mathbf{R}^3$. In Ω_{FEM} we use a finite element mesh $K_h = \{K\}$ with elements K consisting of triangles in $\mathbf{R}^2$ and tetrahedra in $\mathbf{R}^3$. We associate with K_h a mesh function $h = h(x)$ representing the diameter of the element K containing x. For the time discretization we let $J_k = \{J\}$ be a partition of the time interval $I = (0, T)$ into time intervals $J = (t_{k-1}, t_k]$ of uniform length $\tau = t_k - t_{k-1}$.

We define the following L_2 inner product and norm

$$((p, q)) = \int_0^T \int_\Omega pq \, dx \, dt, \quad \|p\|^2 = ((p, p)).$$

We further use the notation $Dv = \frac{\partial v}{\partial t}$.

To formulate the finite element method for (2.3)-(2.4) we introduce the finite element trial space W_h^v and test space W_h^λ defined by :

$$
\begin{aligned}
W_1^v &:= \{v \in H^1(\Omega \times J) : v(\cdot, 0) = 0,\ \partial_n v|_{\Gamma_1} = v_1, \partial_n v|_{\Gamma_2} = 0\},\\
W_2^v &:= \{v \in H^1(\Omega \times J) : v(\cdot, 0) = 0,\ \partial_n v|_{\Gamma} = 0\},\\
W^\lambda &:= \{\lambda \in H^1(\Omega \times J) : \lambda(\cdot, T) = 0,\ \partial_n \lambda|_{\Gamma} = 0\},\\
W_h^v &:= \{v \in W_1^v \cup W_2^v : v|_{K \times J} \in P_1(K) \times P_1(J), \forall K \in K_h, \forall J \in J_k\},\\
W_h^\lambda &:= \{\lambda \in W^\lambda : \lambda|_{K \times J} \in P_1(K) \times P_1(J), \forall K \in K_h, \forall J \in J_k\},
\end{aligned}
$$

where $P_1(K)$ and $P_1(J)$ are the set of linear functions on K and J, respectively.

The finite element method for (2.3)-(2.4) now reads: Find $E_h \in W_h^v$ such that $\forall \bar{\lambda} \in W_h^\lambda$,

$$
-((\epsilon D E_h, D\bar{\lambda})) + ((\frac{1}{\mu} \nabla E_h, \nabla \bar{\lambda})) = ((\frac{1}{\mu} v_1, \bar{\lambda}))_{(0,t_1] \times \Gamma_1}. \tag{3.0}
$$

Here, the initial condition $DE(\cdot, 0) = 0$ is imposed in weak form through the variational formulation.

Expanding E in terms of the standard continuous piecewise linear functions $\varphi_i(x)$ in space and $\psi_i(t)$ in time and substituting this into (3.0), we obtain the following system of linear equations:

$$
\mathbf{M}(\mathbf{E}^{k+1} - 2\mathbf{E}^k + \mathbf{E}^{k-1}) = -\tau^2 \mathbf{K}(\frac{1}{6}\mathbf{E}^{k-1} + \frac{2}{3}\mathbf{E}^k + \frac{1}{6}\mathbf{E}^{k+1}), \quad k = 1, ..., N-1, \tag{3.1}
$$

with initial conditions :

$$
E(\cdot, 0) = DE(\cdot, 0) = 0. \tag{3.2}
$$

Here, $\mathbf{M}$ is the mass matrix in space, $\mathbf{K}$ is the stiffness matrix, $k = 1, 2, 3\ldots$ denotes the time level, $\mathbf{E}$ is the unknown discrete field values of E, and τ is the time step. The explicit formulas for the entries in (3.1) at each element e are given as

$$
\begin{aligned}
M_{i,j}^e &= (\epsilon \varphi_i, \varphi_j)_e,\\
K_{i,j}^e &= (\frac{1}{\mu} \nabla \varphi_i, \nabla \varphi_j)_e.
\end{aligned} \tag{3.3}
$$

To obtain an explicit scheme we approximate $\mathbf{M}$ with the lumped mass matrix $\mathbf{M}^{\mathbf{L}}$, where approximate values of the mass integrals are obtained by using a quadrature rule, see [16, 11]. By multiplying (3.1) with $(\mathbf{M}^{\mathbf{L}})^{-1}$ and replacing the terms $\frac{1}{6}\mathbf{E}^{k-1} + \frac{2}{3}\mathbf{E}^k + \frac{1}{6}\mathbf{E}^{k+1}$ by $\mathbf{E}^k$, we obtain an efficient explicit formulation:

$$
\mathbf{E}^{k+1} = 2\mathbf{E}^k - \tau^2 (\mathbf{M}^{\mathbf{L}})^{-1} \mathbf{K} \mathbf{E}^k - \mathbf{E}^{k-1} \quad k = 1, ..., N-1. \tag{3.4}
$$

In order to keep the same accuracy for the mass-lumped scheme as for the classical scheme (without mass-lumping), we use Gauss-Lobato quadrature rule which is exact for P_1 elements. On a regular mesh, the mass lumping using Gauss-Lobato quadrature rule for P_1 elements provides a second order FDM approximation, or coincides with the FEM approximation. This is particularly important in our case since we are using a hybrid FEM/FDM method.

4 The inverse problem

We formulate the inverse problem for (2.3)-(2.4) as follows: given the function $\partial_n E = v_1$ on $\Gamma_1 \times (0, t_1]$ determine the coefficients $\epsilon(x), \mu(x)$ for $x \in \Omega$ which minimizes the quantity

$$
\begin{aligned}
J(E,\epsilon,\mu) = \frac{1}{2}\int_0^T \int_\Omega (E-\tilde{E})^2 \delta_{obs}\; dxdt \\
+ \frac{1}{2}\gamma_1 \int_\Omega (\epsilon-\epsilon_0)^2 \; dx + \frac{1}{2}\gamma_2 \int_\Omega (\mu-\mu_0)^2 \; dx.
\end{aligned}
\tag{4.1}
$$

Here $\tilde{E}$ is the observed data at a finite set of observation points x_{obs}, E satisfies (2.3)-(2.4) and thus depends on ϵ, μ. Moreover $\delta_{obs} = \sum \delta(x_{obs})$ is a sum of delta-functions $\delta(x_{obs})$ corresponding to the observation points, $\gamma_{i,i=1,2}$, are regularization parameters, and ϵ_0, μ_0 are initial guess values for parameters to be reconstructed. Choosing the regularization parameters can be done iteratively in the computations and is discussed in Section 10.

To solve this minimization problem, we introduce the Lagrangian

$$
L(u) = J(E,\epsilon,\mu) - ((\epsilon DE, D\lambda)) + ((\frac{1}{\mu}\nabla E, \nabla\lambda)) - ((\frac{1}{\mu}v_1, \lambda))_{(0,t_1]\times\Gamma_1}, \tag{4.2}
$$

where $u = (E,\lambda,\epsilon,\mu)$, and search for a stationary point with respect to u satisfying for all $\bar{u} = (\bar{E},\bar{\lambda},\bar{\epsilon},\bar{\mu})$

$$
L'(u;\bar{u}) = 0, \tag{4.3}
$$

where L' is the gradient of L. The equation (4.3) expresses that for all $\bar{u}$,

$$
\begin{aligned}
L'_\lambda(u;\bar{\lambda}) &= -((\epsilon D\bar{\lambda}, DE)) + ((\frac{1}{\mu}\nabla E, \nabla\bar{\lambda})) - ((\frac{2}{\mu}v_1, \bar{\lambda}))_{(0,t_1]\times\Gamma_1} = 0, \\
L'_E(u;\bar{E}) &= ((E-\tilde{E}, \bar{E}))_{\delta_{obs}} - ((\epsilon D\lambda, D\bar{E})) + ((\frac{1}{\mu}\nabla\lambda, \nabla\bar{E})) = 0, \\
L'_\epsilon(u;\bar{\epsilon}) &= -((DED\lambda, \bar{\epsilon})) + \gamma_1(\epsilon-\epsilon_0, \bar{\epsilon}) = 0, \\
L'_\mu(u;\bar{\mu}) &= -((\frac{1}{\mu^2}\nabla\lambda\nabla E, \bar{\mu})) + ((\frac{1}{\mu^2}v_1\lambda, \bar{\mu}))_{(0,t_1]\times\Gamma_1} + \gamma_2(\mu-\mu_0, \bar{\mu}) = 0.
\end{aligned}
\tag{4.4}
$$

The first equation in (4.4) is a weak form of the state equation (2.4), the second equation is a weak form of the adjoint state equation,

$$
\begin{aligned}
\epsilon\frac{\partial^2\lambda}{\partial t^2} - \nabla\cdot(\frac{1}{\mu}\nabla\lambda) = -(E-\tilde{E})\delta_{obs},\; x\in\Omega,\; 0<t<T, \\
\partial_n\lambda = 0 \text{ on } \Gamma\times(0,T), \\
\lambda(\cdot,T) = D\lambda(\cdot,T) = 0 \text{ in } \Omega,
\end{aligned}
\tag{4.5}
$$

and the last two equations expresses stationarity with respect to the parameters ϵ, μ.

5 A finite element method for inverse problem

To formulate a finite element method for (4.3) we introduce the finite element space V_h of piecewise constants for the coefficients $\epsilon(x), \mu(x)$, defined by :

$$
V_h := \{v \in L_2(\Omega) : v \in P_0(K), \forall K \in K_h\}.
$$

Recalling the definition of W_h^v related to the state E and W_h^λ for the costate λ, and defining $U_h = W_h^v \times W_h^\lambda \times V_h \times V_h$, we formulate the finite element method for (4.3) as: Find $u_h \in U_h$, such that

$$
L'(u_h;\bar{u}) = 0 \;\; \forall\bar{u}\in U_h. \tag{5.1}
$$

6 An a posteriori error estimate for the Lagrangian

We follow [7] to present the main steps in the proof of an a posteriori error estimate for the Lagrangian. We start by writing an equation for the error e in the Lagrangian as

$$
\begin{aligned}
e = L(v) - L(v_h) &= \int_0^1 \frac{d}{d\epsilon} L(v\epsilon + (1-\epsilon)v_h) d\epsilon \\
&= \int_0^1 L'(v\epsilon + (1-\epsilon)v_h; v - v_h) d\epsilon = L'(v_h; v - v_h) + R,
\end{aligned}
\tag{6.1}
$$

where R denotes a (small) second order term. For full details of the arguments we refer to [2] and [14].

Using the Galerkin orthogonality (4.3), the splitting

$$
v - v_h = (v - v_h^I) + (v_h^I - v_h) \tag{6.2}
$$

where v_h^I denotes an interpolant of v, and neglecting the term R, we get the following error representation:

$$
e \approx L'(v_h; v - v_h^I). \tag{6.3}
$$

For full details of the derivation of an a posteriori error estimate for the Lagrangian for the time-dependent scalar wave equation, we refer to [4, 6, 7]. The main steps of the derivation are: estimation of $v - v_h^I$ in terms of derivatives of v, the mesh parameter h and time step τ. Then the derivative of v is estimated by the corresponding derivatives of v_h. The concrete form of the a posteriori error estimate (6.3) for the error in Lagrangian (4.2) is:

$$
\begin{aligned}
\left|e\right| \leq\ & ((R_{E_1}, \sigma_\lambda))_{(0,t_1]\times\Gamma_1} + ((R_{E_2}, \sigma_\lambda)) + ((R_{E_3}, \sigma_\lambda)) \\
& + ((R_{\lambda_1}, \sigma_E)) + ((R_{\lambda_2}, \sigma_E)) + ((R_{\lambda_3}, \sigma_E)) \\
& + ((R_{\epsilon_1}, \sigma_\epsilon)) + (R_{\epsilon_2}, \sigma_\epsilon) \\
& + ((R_{\mu_1}, \sigma_\mu)) + ((R_{\mu_2}, \sigma_\mu))_{(0,t_1]\times\Gamma_1} + (R_{\mu_3}, \sigma_\mu),
\end{aligned}
\tag{6.4}
$$

where the residuals are defined by

$$
\begin{aligned}
R_{E_1} &= \frac{2}{\mu_h}|v_1|, R_{E_2} = \max_{S\subset\partial K} \frac{1}{\mu_h} h_k^{-1}\left|\left[\partial_s E_h\right]\right|,\ R_{E_3} = \epsilon_h \tau^{-1}\left|\left[\partial E_{ht}\right]\right|, \\
R_{\lambda_1} &= |E_h - \tilde{E}|_{\delta_{obs}}, R_{\lambda_2} = \max_{S\subset\partial K} \frac{1}{\mu_h} h_k^{-1}\left|\left[\partial_s \lambda_h\right]\right|,\ R_{\lambda_3} = \epsilon_h \tau^{-1}\left|\left[\partial \lambda_{ht}\right]\right|, \\
R_{\epsilon_1} &= |D\lambda_h| \cdot |DE_h|,\ R_{\epsilon_2} = \gamma_1|\epsilon_h - \epsilon_0|, \\
R_{\mu_1} &= \frac{1}{\mu_h^2}|\nabla\lambda_h| \cdot |\nabla E_h|,\ R_{\mu_2} = \frac{1}{\mu_h^2}|v_1| \cdot |\lambda_h|,\ R_{\mu_3} = \gamma_2|\mu_h - \mu_0|,
\end{aligned}
$$

and the interpolation errors are

$$
\begin{aligned}
\sigma_\lambda &= C\tau\left|\left[\frac{\partial \lambda_h}{\partial t}\right]\right| + Ch\left|\left[\frac{\partial \lambda_h}{\partial n}\right]\right|, \\
\sigma_E &= C\tau\left|\left[\frac{\partial E_h}{\partial t}\right]\right| + Ch\left|\left[\frac{\partial E_h}{\partial n}\right]\right|, \\
\sigma_\epsilon &= C\left|[\epsilon_h]\right|, \\
\sigma_\mu &= C\left|[\mu_h]\right|.
\end{aligned}
$$

Here, $[v]$ denotes the maximum of the modulus of the jump on element K (or time interval J) of the v across a face of K (or boundary node of J), $[\partial_s v]$ denotes the maximum modulus of a jump in the normal derivative of v across a side K, $[\partial_t v]$ is the maximum modulus of the jump of the time derivative of v across a boundary node of J, C is the interpolation constant of moderate size.

7 A posteriori error estimation for parameter identification

Following [8] we present more general a posteriori error estimation to estimate error in the reconstructed parameter. We first note that

$$
\begin{aligned}
L'(u;\tilde{u}) - L'(u_h;\tilde{u}) &= \int_0^1 \frac{d}{d\epsilon} L'(u\epsilon + (1-\epsilon)u_h;\tilde{u})d\epsilon \\
&= \int_0^1 L''(u\epsilon + (1-\epsilon)u_h; u-u_h, \tilde{u})d\epsilon \\
&= L''(u_h; u-u_h, \tilde{u}) + R,
\end{aligned}
$$

where R is a second order remainder and $L''(u_h;\cdot,\cdot)$ is the Hessian of the Lagrangian. Since $L'(u;\tilde{u}) = 0$ and using the Galerkin orthogonality (5.1) with a splitting $\tilde{u} - \tilde{u}_h = (\tilde{u} - \tilde{u}_h^I) + (\tilde{u}_h^I - \tilde{u}_h)$ where $\tilde{u}_h^I \in U_h$ denotes an interpolant of $\tilde{u}$, we get the following equation:

$$-L''(u_h; u-u_h, \tilde{u}) = L'(u_h;\tilde{u}) + R = L'(u_h;\tilde{u} - \tilde{u}_h^I) + R. \tag{7.1}$$

Estimate of the error in the parameter identification involve solution to the dual problem

$$-L''(u_h; u-u_h, \tilde{u}) = (\psi, u-u_h), \tag{7.2}$$

where ψ is a given data. Comparing (7.1) with (7.2) and neglecting term R in (7.1) we get the analog of an a posteriori error estimate for Lagrangian

$$(\psi, u-u_h) \approx L'(u_h;\tilde{u} - \tilde{u}_h^I), \tag{7.3}$$

where u is replaced by $\tilde{u}$. From this estimate we observe that the form of the error for a parameter identification is similar to the error in the Lagrangian with u replaced by $\tilde{u}$ in weights.

We can choose $\bar{u} = u - u_h$ in (7.2) and the dual problem can be written as:

$$-L''(u_h;\bar{u},\tilde{u}) = (\psi,\bar{u}). \tag{7.4}$$

We conclude that for appropriate choice of ψ as data in the dual problem and solving approximately of (7.4) for $\tilde{u}$ we can get values of the error for $\bar{u}$.

8 The Hessian of the Lagrangian

Now we present the Hessian of the Lagrangian for the problem (2.3)-(2.4). The corresponding Lagrangian for (2.3)-(2.4) in the case $\mu = 1$ is

$$L(u) = J(E,\epsilon) - ((\epsilon DE, D\lambda)) + ((\nabla E, \nabla\lambda)) - ((v_1,\lambda))_{(0,t_1]\times\Gamma_1}, \tag{8.1}$$

where $u = (E,\lambda,\epsilon)$. The Hessian of the Lagrangian (8.1) then takes the following form:

$$L''(u;\bar{u},\tilde{u}) = L''_E(u;\bar{u},\tilde{E}) + L''_\lambda(u;\bar{u},\tilde{\lambda}) + L''_\epsilon(u;\bar{u},\tilde{\epsilon}), \tag{8.2}$$

where

$$L''_E(u;\bar{u},\tilde{E}) = -((\epsilon D\bar{\lambda}, D\tilde{E})) + ((\nabla\tilde{E},\nabla\bar{\lambda})) + ((\tilde{E},\bar{E}))_{\delta_{obs}} - ((D\tilde{E}D\lambda,\bar{\epsilon})),$$
$$L''_\lambda(u;\bar{u},\tilde{\lambda}) = -((\epsilon D\bar{E}, D\tilde{\lambda})) + ((\nabla\tilde{\lambda},\nabla\bar{E})) - ((v_1,\tilde{\lambda}))_{(0,t_1]\times\Gamma_1} - ((DED\tilde{\lambda},\bar{\epsilon})),$$
$$L''_\epsilon(u;\bar{u},\tilde{\epsilon}) = -((DED\bar{\lambda},\tilde{\epsilon})) - ((D\lambda D\bar{E},\tilde{\epsilon})) + \gamma_1(\bar{\epsilon},\tilde{\epsilon}).$$

Here we used the boundary conditions $\partial_n\lambda = \partial_n\bar{\lambda} = \partial_n\tilde{\lambda} = 0$ and $\partial_n E = \partial_n\bar{E} = \partial_n\tilde{E} = v_1|_{(0,t_1]\times\Gamma_1}$. Then the dual problem (7.4) takes the following strong form:

$$\begin{aligned}
\epsilon\frac{\partial^2\tilde{\lambda}}{\partial t^2} - \nabla\cdot(\nabla\tilde{\lambda}) + \tilde{E}_{\delta_{obs}} + \tilde{\epsilon}\frac{\partial^2\lambda}{\partial t^2} &= \psi_1,\\
\epsilon\frac{\partial^2\tilde{E}}{\partial t^2} - \nabla\cdot(\frac{1}{\epsilon}\nabla\tilde{E}) + \tilde{\epsilon}\frac{\partial^2 E}{\partial t^2} - v_1|_{(0,t_1]\times\Gamma_1} &= \psi_2,\\
-\int_0^T D\lambda D\tilde{E}dt - \int_0^T D\tilde{\lambda}DEdt + \gamma_1\tilde{\epsilon} &= \psi_3
\end{aligned} \tag{8.3}$$

with initial and boundary conditions. Our goal is to solve the system (8.3) with already known approximation to the final solution u, computed using adaptive algorithm in Section 9, and find $\tilde{u} = (\tilde{E},\tilde{\lambda},\tilde{\epsilon})$. We assume that the solution of the adjoint problem, λ, and $\nabla\lambda$ will be small, and we can neglect all the terms involving λ to get the following approximated problem:

$$\begin{aligned}
\epsilon\frac{\partial^2\tilde{\lambda}}{\partial t^2} - \nabla\cdot(\nabla\tilde{\lambda}) + \tilde{E}_{\delta_{obs}} &= \psi_1,\\
\epsilon\frac{\partial^2\tilde{E}}{\partial t^2} - \nabla\cdot(\nabla\tilde{E}) + \tilde{\epsilon}\frac{\partial^2 E}{\partial t^2} - v_1|_{(0,t_1]\times\Gamma_1} &= \psi_2,\\
-\int_0^T D\tilde{\lambda}DEdt + \gamma_1\tilde{\epsilon} &= \psi_3.
\end{aligned} \tag{8.4}$$

As already mentioned in [8], the stability properties of this system is an open problem.

To solve the problem (8.4) we use the iterative algorithm described in [8], with already computed approximation to u (values $u_h = (E_h,\lambda_h,\epsilon_h)$, obtained in an adaptive algorithm in Section 9), and with initial guess $\tilde{u} = \tilde{u}^m, m = 0$. From the last equation in (8.4) we can update $\tilde{\epsilon}$ as the iterative procedure

$$\tilde{\epsilon}^{m+1} = \tilde{\epsilon}^m + \alpha(\psi_3 + \int_0^T D\tilde{\lambda^m}DE_h dt - \gamma_1\tilde{\epsilon}^m), \tag{8.5}$$

where $\alpha > 0$ is the step length in the iterative procedure. Next, we solve the second equation in (8.4) to find $\tilde{E}$, and finally, the first equation to find $\tilde{\lambda}$. We stop computations when $||\tilde{\epsilon}^{m+1} - \tilde{\epsilon}^m|| < eps$, where $eps > 0$ is a tolerance, otherwise, we choose $\tilde{\epsilon}^m = \tilde{\epsilon}^{m+1}$ and return to the iterative procedure (8.5).

9 An adaptive algorithm for solution of the inverse problem

To improve the reconstruction and achieve better convergence in the computed parameter ϵ ($\mu = 1$), we use the following adaptive algorithm:

0. Choose an initial mesh K_h and an initial time partition J_0 of the time interval $(0,T)$. Starting from initial guess of the parameter ϵ^0, compute a sequence of ϵ^n in the following steps:

1. Compute the solution E^n of the forward problem (2.3)-(2.4) on K_h and J_k with $\epsilon = \epsilon^{(n)}$.

2. Compute the solution λ^n of the adjoint problem (4.5) on K_h and J_k.

3. Update the parameter ϵ on K_h and J_k using the quasi-Newton method

$$\epsilon^{n+1} = \epsilon^n + \alpha^n H^n g^n, \tag{9.1}$$

where H^n is an approximate Hessian, computed using the usual BFGS update formula for the Hessian, see [18]. Next, g^n is the gradient of the Lagrangian (4.2) with respect to the parameter ϵ:

$$g^n = -\int_0^T D\lambda^n DE^n dt + \gamma_1(\epsilon^n - \epsilon_0), \tag{9.2}$$

and α is the step length in the parameter upgrade computed using an one-dimensional search algorithm [19].

4. Stop if the gradient $g^n < tol$; if not, set $n = n + 1$ and go to step 5.

5. Compute an a posteriori error estimate (6.4) and refine all elements where $|e| > tol$. Here tol is a tolerance chosen by the user.

6. Construct a new mesh K_h and a new time partition J_k. Return to step 1 and perform all steps of the optimization algorithm on a new mesh.

As we see from (6.4), the error in the Lagrangian consists of space-time integrals of different residuals multiplied by the interpolation errors. Thus, to estimate the error in the Lagrangian we need to compute the approximated values of $(E_h, \lambda_h, \epsilon_h)$ together with residuals and interpolation errors. Since the residuals $R_{\epsilon_1}, R_{\epsilon_2}$ dominate we neglect computations of all the other residuals in the a posteriori error estimator and compute the a posteriori error in step 5 of the adaptive algorithm as

$$(R_{\epsilon_1} + R_{\epsilon_2})\sigma_\epsilon > tol. \tag{9.3}$$

In the current work, the refinement is based on the residuals, since they already give good indications of where to refine the mesh. The interpolation errors and thus exact value of the computational error in the already reconstructed parameter can be obtained by computing the Hessian of the Lagrangian using the iterative procedure in Section 8.

We should note that the regularization parameter should be small and not disturb the reconstruction by too much regularization. The value of γ will depend on the actual values of the reconstructed parameter ϵ.

10 Numerical Results

In this section we present several numerical examples to show performance of the adaptive hybrid method and the usefulness of the a posteriori error estimator (6.4).

The computational domain in all our tests $\Omega = \Omega_{FEM} \cup \Omega_{FDM}$ is set as $\Omega = [-4.0, 4.0] \times [-5.0, 5.0]$, which is split into a finite element domain $\Omega_{FEM} = [-3.0, 3.0] \times [-3.0, 3.0]$ with an unstructured mesh and a surrounding domain Ω_{FDM} with a structured mesh, see Fig. 2. The space mesh in Ω_{FEM} consists of triangles and in Ω_{FDM} of squares, with mesh size in the overlapping regions $h = 0.25$ and $h = 0.125$, in Example 1 and Example 2, correspondingly.

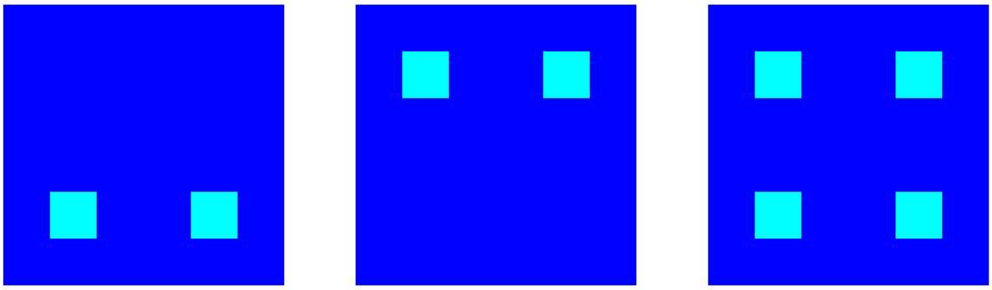

(a) Ω_l (b) Ω_h (c) Ω_{FEM}

Figure 1: We show the square lattice of a crystal where the material to be reconstructed is a square lattice of columns.

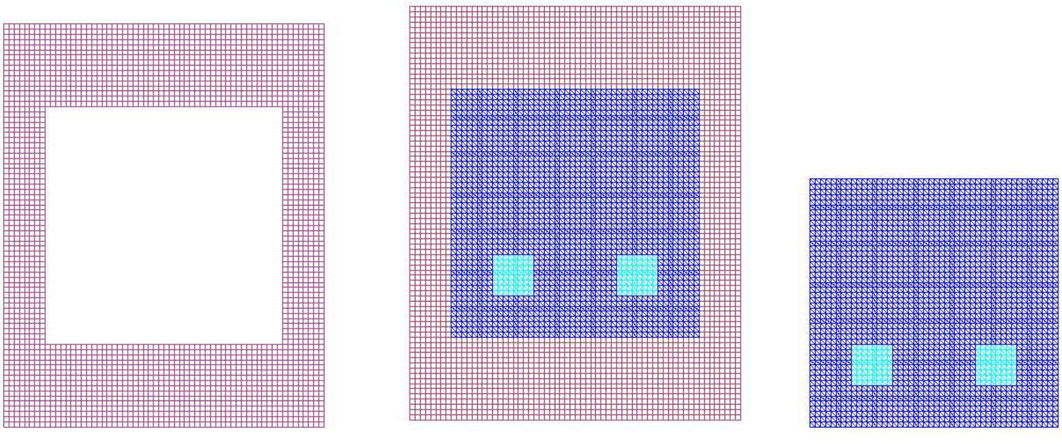

(a) Ω_{FDM} (b) $\Omega = \Omega_{FEM} \cup \Omega_{FDM}$ (c) Ω_{FEM}

Figure 2: The hybrid mesh (b) is a combinations of a structured mesh (a), where FDM is applied, and a mesh (c), where we use FEM, with a thin overlapping of structured elements.

opt.it.	625 nodes	809 nodes	1263 nodes	2225 nodes
1	0.0118349	0.0108764	0.0108764	0.010476
2	0.0095824	0.00987447	0.00965067	0.00954041
3	0.00822312	0.00709372	0.00558728	0.00769998
4	0.00748565	0.00318215	0.00273809	0.00313069
5	0.00619674	0.00291434		
6	0.00528474			
7	0.00471419			
8	0.00354939			

Table 1: $||E - E_{obs}||$ on the adaptively refined meshes in the reconstruction of the lower columns in square lattice. Number of stored corrections in quasi-Newton method is $m = 15$. Computations was performed with noise level $\sigma = 0$ and regularization parameter $\gamma = 0.1$.

We apply the hybrid finite element/difference method presented in [9] where finite elements are used in Ω_{FEM} and finite differences in Ω_{FDM}. At the top and bottom boundaries of Ω we use first-order absorbing boundary conditions [13]. At the lateral boundaries, mirror boundary conditions allow us to assume an infinite space-periodic crystal in the lateral direction.

For simplicity, we assume that material is nonmagnetic, or $\mu = 1$ in Ω, and $\epsilon = \mu = 1$ in Ω_{FDM}. Thus, we need only to reconstruct electric permittivity ϵ in Ω_{FEM}.

First we present tests on reconstruction of the parameter ϵ inside the domains Ω_l and Ω_h, see Fig. 1-a), b), respectively, and then we present computational results on the reconstruction of the structure of the photonic crystal given in Fig. 1-c).

10.1 Example 1

We start to test the adaptive finite element/difference method on the reconstruction of the structures given in Fig. 1-a), b), where our goal is to find the parameter ϵ in the small square lattices inside the domains Ω_l and Ω_h, respectively.

We solve the forward problem (2.3)-(2.4) with a plane wave pulse given as

$$\partial_n E\big|_{\Gamma_1} = ((\sin(\omega t - \pi/2) + 1)/10), \;\; 0 \leq t \leq \frac{2\pi}{\omega}. \tag{10.1}$$

The field initiates at the boundary Γ_1 - in our examples this boundary represents the top boundary of the computational domain - and propagates in normal direction n into Ω in time $t = (0, T)$. The trace of the forward problem is measured at the observation points which are placed on the lower boundary of the computational domain Ω_{FEM}.

To generate the data at the observation points, we solve the forward problem (2.3)-(2.4) with a plane wave (10.1) in the time interval $t = (0, T)$ with $T = 10.0$ and with the exact value of the parameter $\epsilon = 10.0$ inside the square lattices and $\epsilon = 1.0$ everywhere else. Since the explicit scheme (3.4) is used for solution of the forward and adjoint problems, we chose a time step τ according to the Courant-Friedrich's-Levy (CFL) stability condition to provide a stable time discretization.

We start the adaptive algorithm in Section 9 with guess values of the parameter $\epsilon = 1.0$ at all points in the computational domain Ω_{FEM} and with regularization parameter $\gamma = 0.1$.

To reconstruct the lower and upper square lattices in Ω_{FEM} the computations were performed on the four adaptively refined meshes shown in Fig. 3-a)-d) and Fig. 4-a)-d), respectively. The meshes was refined by computing the residual in the reconstructed parameter ϵ using the adaptive algorithm.

Table 1 shows computed L_2-norms of $||E - E_{obs}||_{L_2}$ for the best value of the reconstructed parameter ϵ in lower square lattices with $\omega = 25$ in (10.1). We present norms on different

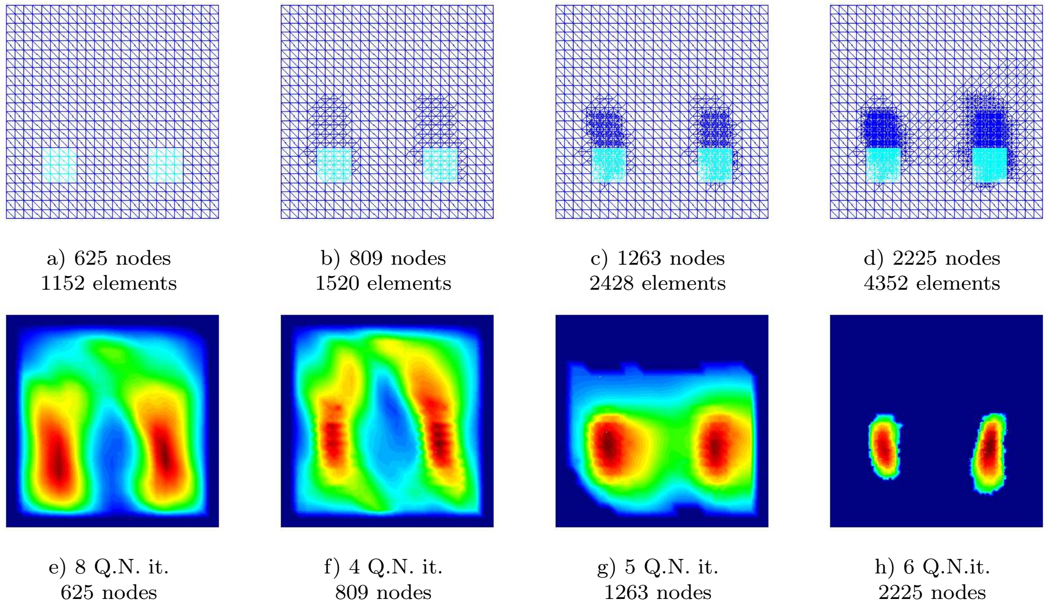

Figure 3: a)-d) Adaptively refined meshes in the reconstruction of the lower square lattices; e)-h) Reconstructed parameter $\epsilon(x)$ on the correspondingly refined meshes at the final optimization iteration computed with $\omega = 25$ and noise level 5% in the observed data.

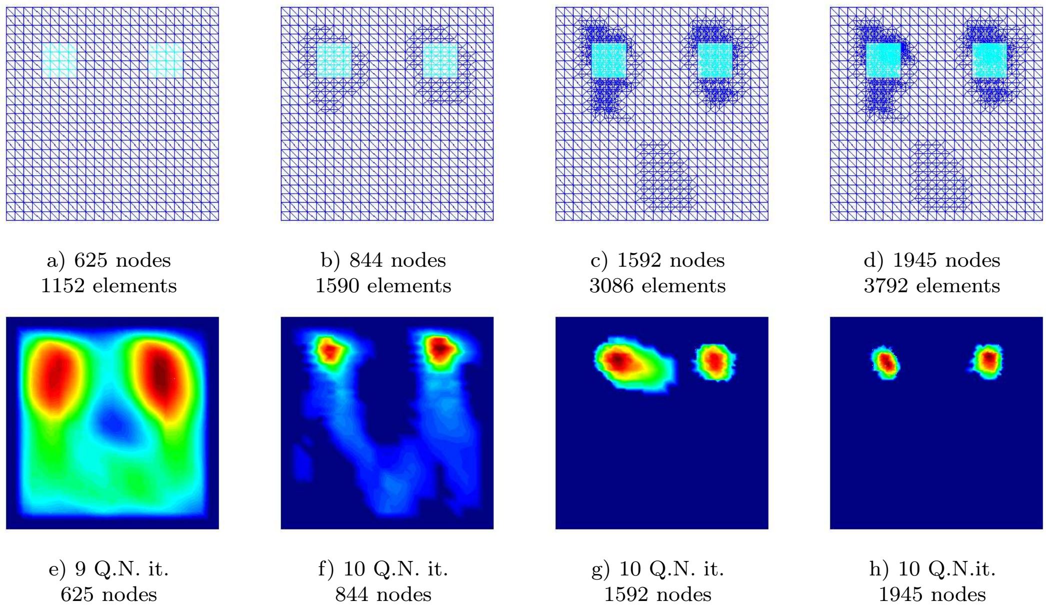

Figure 4: a)-d) Adaptively refined meshes in the reconstruction of the upper square lattices; e)-h) Reconstructed parameter $\epsilon(x)$ on the correspondingly refined meshes at the final optimization iteration computed with $\omega = 25$ and noise level 5% in the observed data.

σ, γ	10^{-5}	10^{-4}	10^{-3}	10^{-2}	10^{-1}
0	0.00630036	0.00630536	0.00475773	0.0046071	0.00313069
1	0.00650122	0.00642409	0.00489691	0.00425432	0.00317147
3	0.00671315	0.00644934	0.00572624	0.00427946	0.00317955
5	0.0068622	0.00661597	0.00639352	0.00428971	0.00318703
7	0.00731985	0.00598225	0.00631647	0.00462458	0.00312281
10	0.00672832	0.00618862	0.00673036	0.00467998	0.00331152
20	0.00702925	0.00696454	0.00640261	0.00448304	0.0037926

Table 2: $||E - E_{obs}||$ for the best reconstruction of the lower columns in the square lattice. We present results for different noise levels σ and regularization parameters γ.

σ, γ	10^{-5}	10^{-4}	10^{-3}	10^{-2}	10^{-1}
0	0.00548847	0.00549544	0.00549544	0.00512397	0.00340977
1	0.00547518	0.00549755	0.00489691	0.0055677	0.00345097
3	0.00545709	0.00550747	0.00572624	0.0055182	0.0040041
5	0.00548414	0.00548424	0.00639352	0.0055076	0.00357293
7	0.00544183	0.00544645	0.00631647	0.00552189	0.00353966
10	0.00543398	0.00548045	0.00673036	0.00552947	0.00430008
20	0.00561054	0.00561999	0.00640261	0.00566159	0.00386997

Table 3: $||E - E_{obs}||$ for the best reconstruction of the upper columns in the square lattice. We present results for different noise levels σ and regularization parameters γ.

adaptively refined meshes at each optimization iteration as long as the norms decrease. The computational tests show that the best results are obtained on a finest mesh, where $||E - E_{obs}||$ is reduced approximately by a factor four between first and last optimization iterations.

We performed tests again with adding relative noise to the observed data. The relative disturbation, or noise, in data, E_σ, is computed by adding relative error to computed data E_{obs} using expression

$$E_\sigma = E_{obs} + \alpha(E_{max} - E_{min})\sigma/100. \tag{10.2}$$

Here, α is an random number on the interval $[-1; 1]$, E_{max} and E_{min} are maximal and minimal value of the computed data E_{obs}, and σ is noise in percents.

Using the results in Tables 2, 3 we can conclude that we have still good reconstruction for the parameter ϵ in optimization method even with noise in the data. Fig. 3-e)-h) and Fig. 4-e)-h) confirm obtained results where we show the reconstructed parameter ϵ at the final optimization iteration computed with $\omega = 25$ and noise level 5% in the observed data. We show the parameter field $\epsilon(x)$, indicating domains with a given parameter value. We see that although the qualitative reconstruction on the coarse grid already allows the recovery of the location of the square lattices from limited boundary data, the quantitative reconstruction becomes acceptable only on the refined grids.

Fig. 5 presents comparisons of the L_2-norms in space in the reconstruction of the lower square lattices of the adjoint problem solution λ_h over the time interval $(0, 10.0)$. We show norms on different optimization iterations on the mesh with 2225 nodes without and with adding 7% noise in the data. We observe that norms decreases with an increasing number of optimization iterations as it should. We also note that the behavior of the adjoint problem solution is stable to small perturbation in the data. Fig. 6 shows similar results for reconstruction of the upper square lattices.

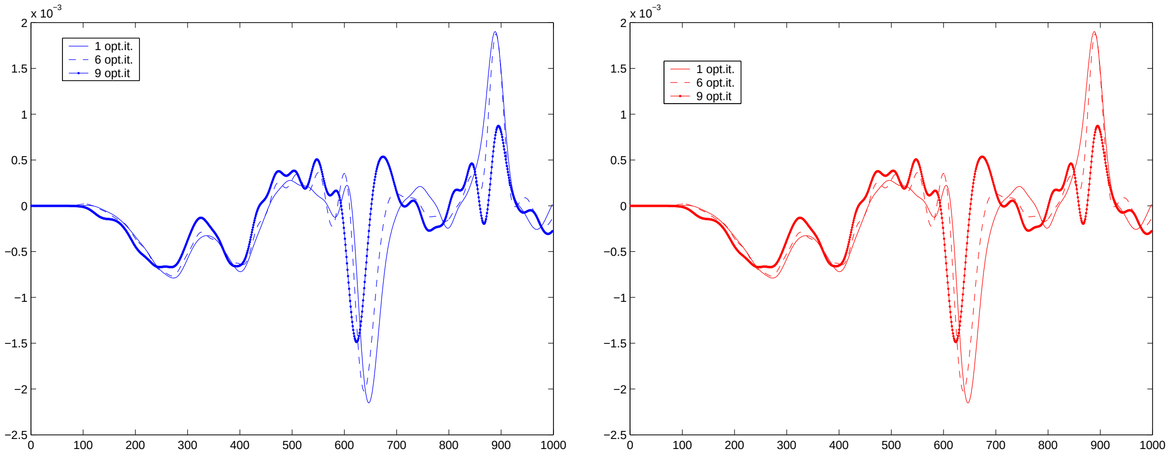

noise $\sigma = 7\%$ noise $\sigma = 0\%$

Figure 5: L_2-norms in space of the adjoint problem solution λ_h in reconstruction of the lower columns in square lattice on different optimization iterations. Here the x-axis denotes time steps on $(0, 10.0)$.

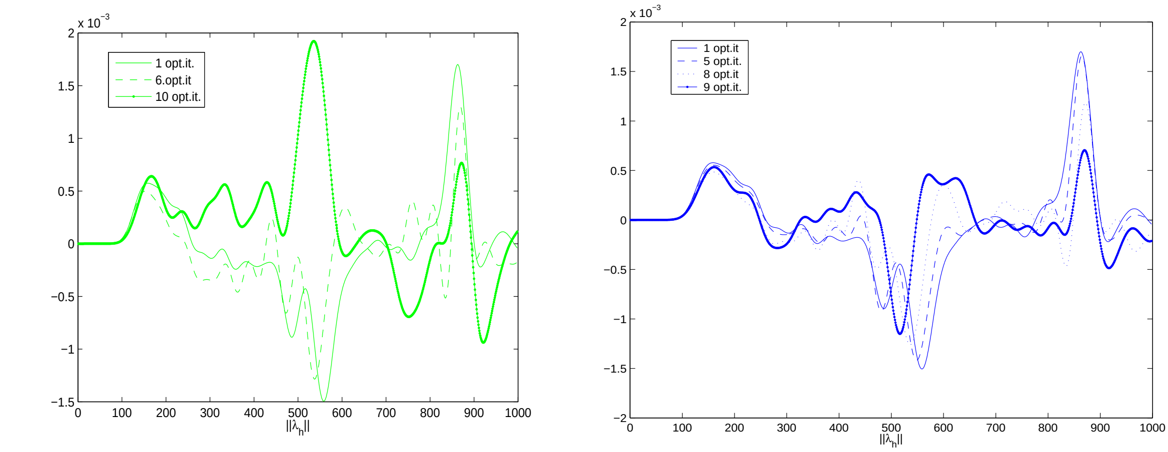

noise $\sigma = 7\%$ noise $\sigma = 0\%$

Figure 6: L_2-norms in space of the adjoint problem solution λ_h in the reconstruction of the upper columns in the square lattice on different optimization iterations. Here the x-axis denotes time steps on $(0, 10.0)$.

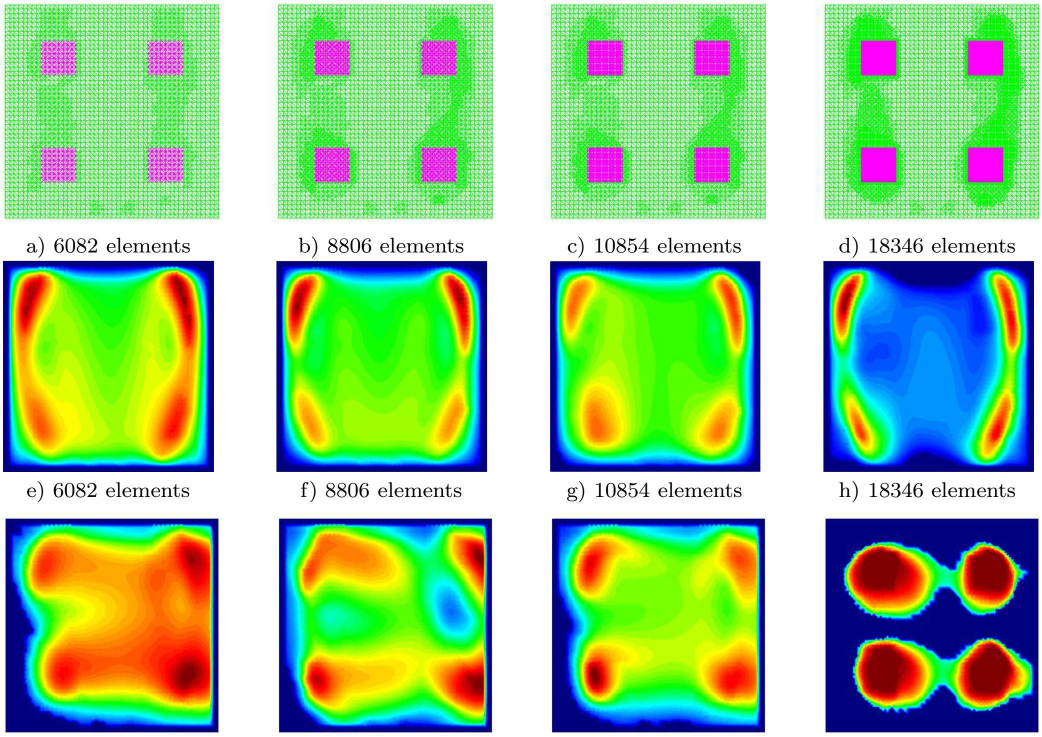

a) 6082 elements b) 8806 elements c) 10854 elements d) 18346 elements

e) 6082 elements f) 8806 elements g) 10854 elements h) 18346 elements

i) 6082 elements j) 8806 elements k) 10854 elements l) 18346 elements

Figure 7: a)-d) Adaptively refined meshes ; e)-h) Reconstructed parameter $\epsilon(x)$, indicating domains with a given parameter value: red color corresponds to the maximum parameter value on the corresponding meshes, and blue color - to the minimum.

10.2 Example 2

Now we seek to reconstruct the structure of the two-dimensional photonic crystal given in Fig. 1-c). The electric field initiates at the top boundary of the computational domain Ω_{FDM} and consists of a plane wave E given as in (10.1) - and propagates in normal direction n into Ω in time $t = (0, 12.0)$ with $\omega = 6$.

First we performed tests when the trace of the forward problem is measured at the observation points only on the lower boundary, and then - tests when the reflected trace is also measured on the lower and top boundaries of the computational domain Ω_{FEM}.

To achieve better results in the reconstruction, we performed tests letting the incoming wave from the top boundary of Ω_{FDM} be equal to the reflected non-plane measured wave from the lower boundary Ω_{FDM}. Thus, to generate the data at the observation points, first we solve the forward problem (2.3)-(2.4) with a plane wave (10.1) in the time interval $t = (0, T)$ with the exact value of the parameter $\epsilon = 4.0$ inside the square lattices and $\epsilon = 1.0$ everywhere else, and values of the solution of the forward problem are registered at the lower boundary of the Ω_{FDM}. Then, using these registered values at the lower boundary, a non-plane wave is initialized in the time interval $t = (T, 2T)$. Again, a time step τ is chosen according to CFL stability condition.

10.2.1 Test1

First we performed tests when the trace of the incoming wave was measured at the observation points at the lower boundary of Ω_{FEM} in time $(0, T)$, and then at the observation points at the top boundary in time $(T, 2T)$.

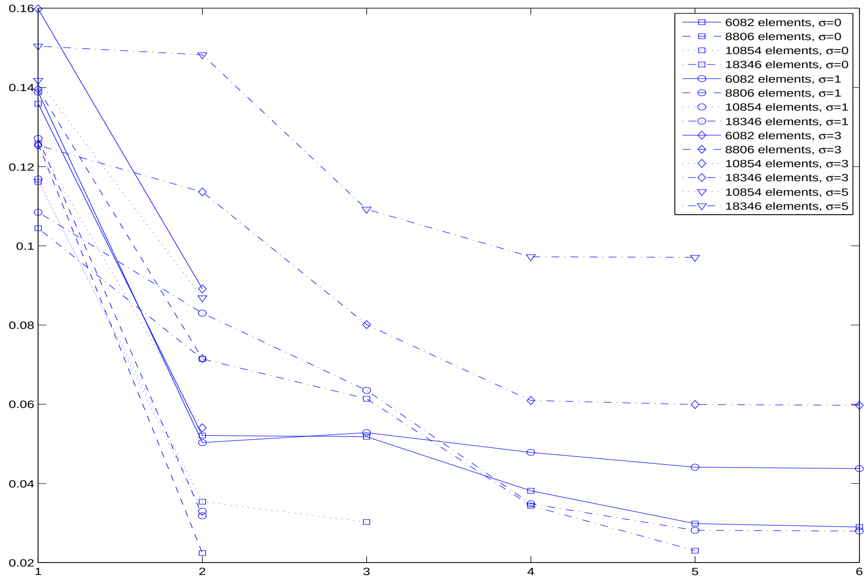

Figure 8: $||E - E_{obs}||$ on adaptively refined meshes. Computations was performed with noise level $\sigma = 0, 1, 3$ and 5% and with regularization parameter $\gamma = 0.01$. Here the x-axis denotes number of optimization iterations.

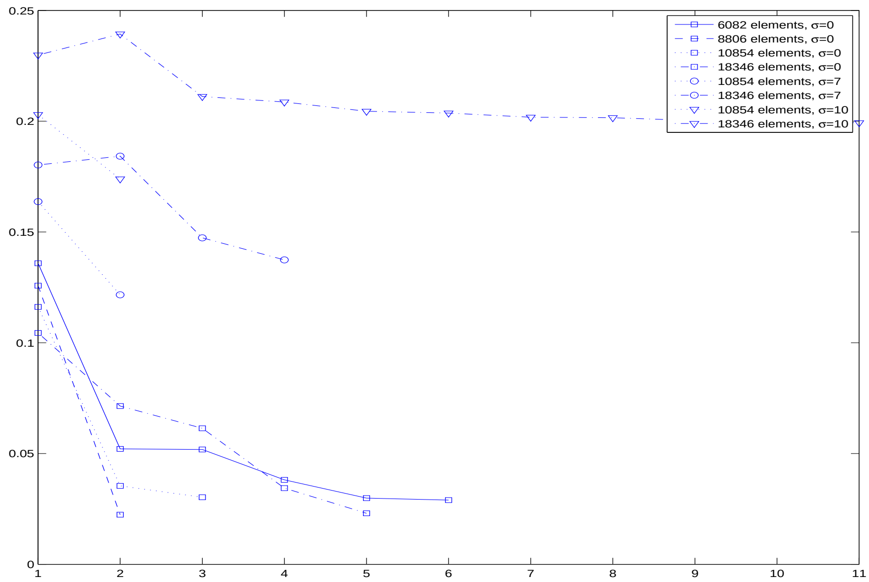

Figure 9: $||E - E_{obs}||$ on adaptively refined meshes. Computations was performed with noise level $\sigma = 0, 7$ and 10% and with regularization parameter $\gamma = 0.01$. Here the x-axis denotes number of optimization iterations.

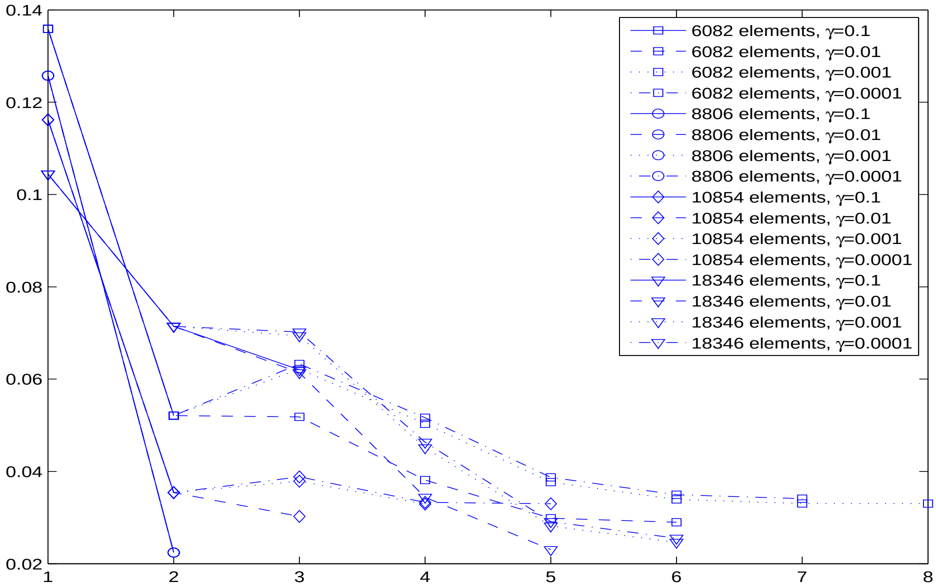

Figure 10: $||E - E_{obs}||$ on adaptively refined meshes. Computations was performed with noise level $\sigma = 0\%$, and with regularization parameters $\gamma = 0.1, 0.01, 0.001, 0.0001$, Here the x-axis denotes number of optimization iterations.

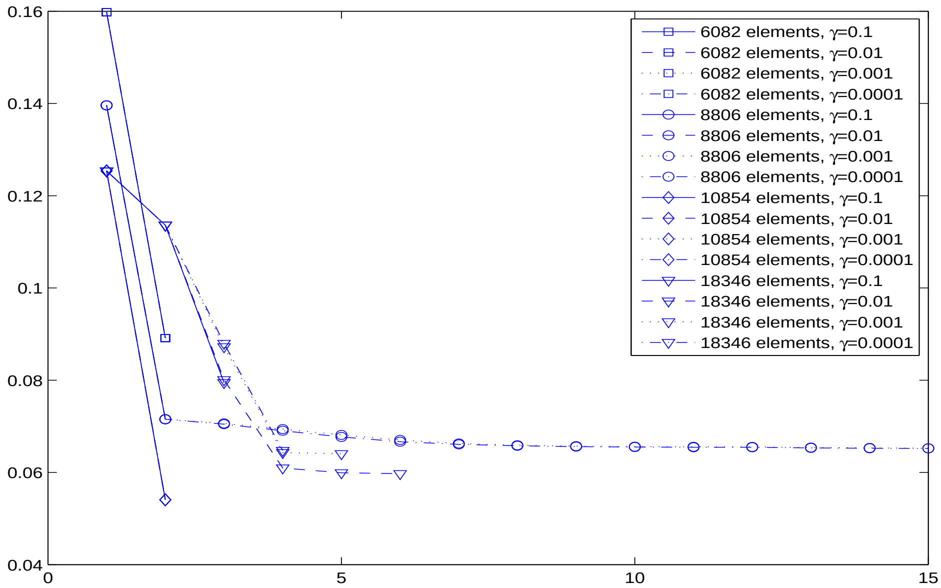

Figure 11: $||E - E_{obs}||$ on adaptively refined meshes. Computations was performed with noise level $\sigma = 3\%$, and with regularization parameters $\gamma = 0.1, 0.01, 0.001, 0.0001$, Here the x-axis denotes number of optimization iterations.

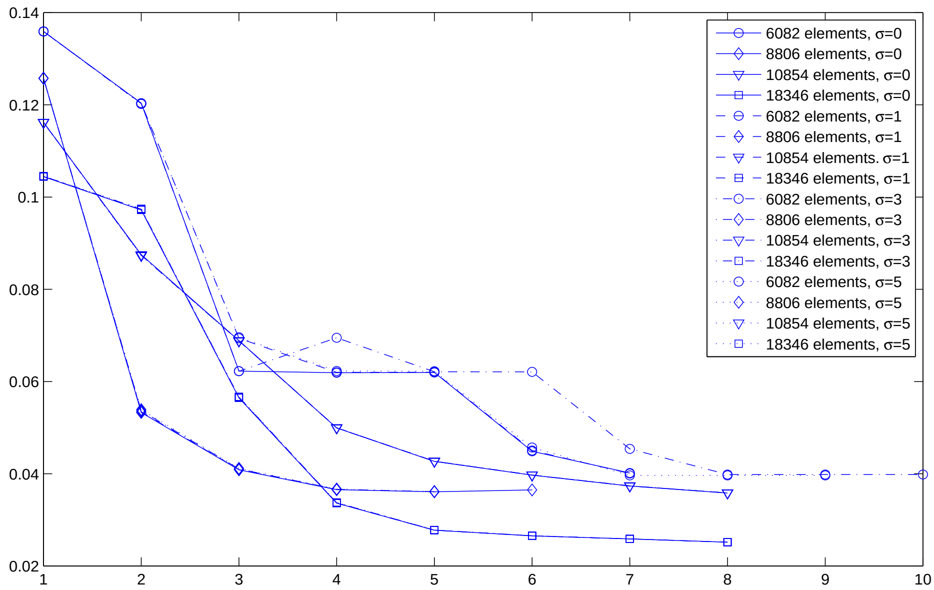

Figure 12: $||E - E_{obs}||$ on adaptively refined meshes. Computations was performed with noise level $\sigma = 0, 1, 3$ and 5% and with regularization parameter $\gamma = 0.01$. Here the x-axis denotes number of optimization iterations.

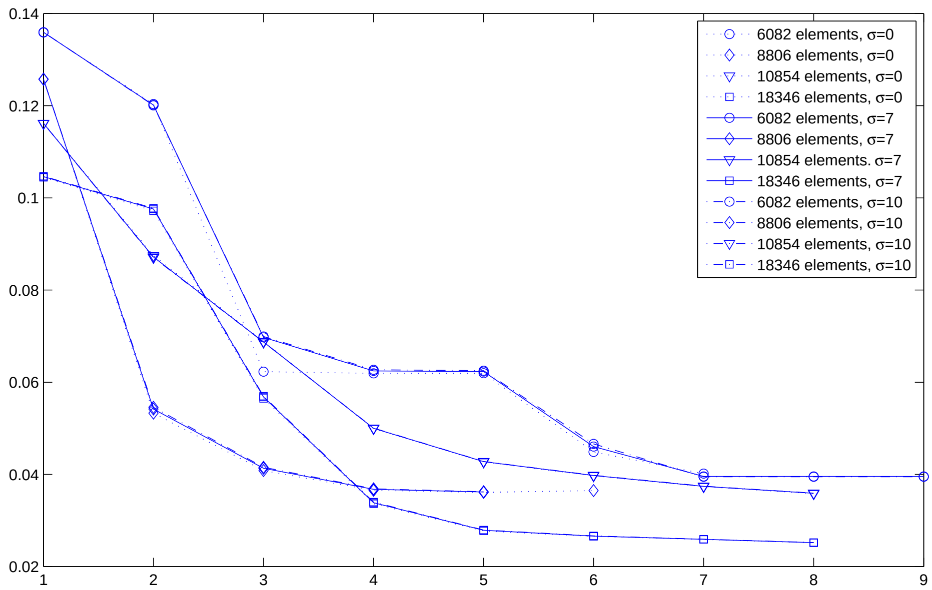

Figure 13: $||E - E_{obs}||$ on adaptively refined meshes. Computations was performed with noise level $\sigma = 0, 7$ and 10% and with regularization parameter $\gamma = 0.01$. Here the x-axis denotes number of optimization iterations.

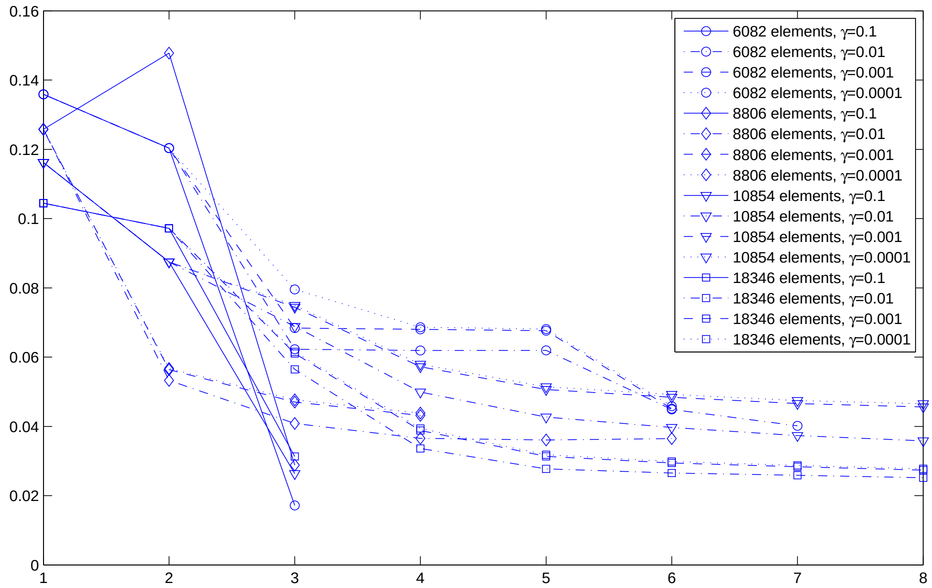

Figure 14: $||E - E_{obs}||$ on adaptively refined meshes. We show computational results with noise level $\sigma = 1\%$ and with regularization parameters $\gamma = 0.1, 0.01, 0.001, 0.0001$. Here the x-axis denotes number of optimization iterations.

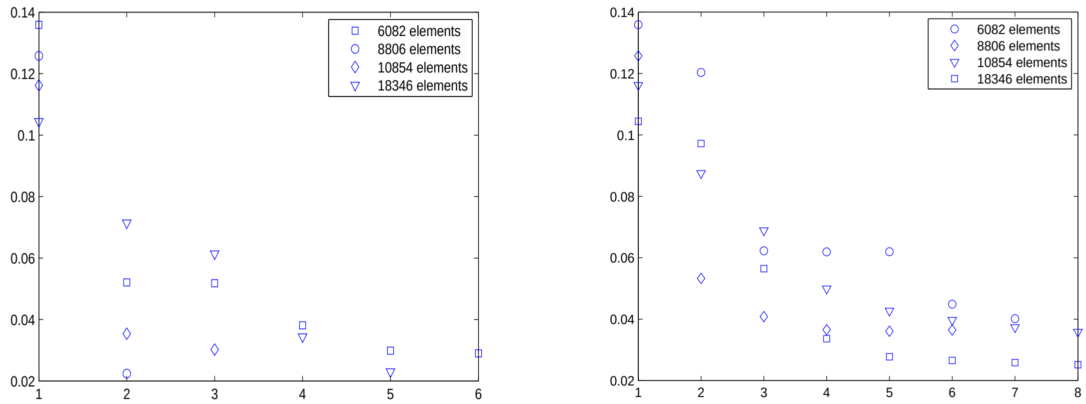

a) b)

Figure 15: $||E - E_{obs}||$ on adaptively refined meshes. We show computations: on a) with noise level $\sigma = 0\%$ and with regularization parameter $\gamma = 0.01$ for Test 1; on b) with noise level $\sigma = 1\%$ and with regularization parameter $\gamma = 0.01$ for Test 2. Here the x-axis denotes number of optimization iterations.

In Fig. 8-9 we present a comparison of the computed L_2-norms of $||E-E_{obs}||_{L_2}$ depending on the relative noise σ on different adaptively refined meshes while the norms decrease. Relative noise σ in the data is computed using the expression (10.2). From these results we conclude that the reconstruction is stable with small values of the noise (see Fig. 8), and unstable with adding more than 5% noise to the data (Fig. 9).

In Fig. 10-11 we show a comparison of the computed L_2-norms of $||E-E_{obs}||_{L_2}$ depending on the different regularization parameters γ. We see that we obtain the smallest value of the difference $||E-E_{obs}||_{L_2}$ with regularization parameter $\gamma = 0.01$ while choosing $\gamma = 0.1$ is too large and involve too much regularization. The computational tests show that the best results are obtained on the finest mesh, where $||E - E_{obs}||$ is reduced approximately by a factor seven between first and last optimization iterations. Fig. 7-e)-h) shows the corresponding to Fig. 15-a) reconstructed parameter field $\epsilon(x)$ at the final optimization iteration indicating domains with a given parameter value.

10.2.2 Test2

Tests, described in this section, was performed when the reflected trace of the incoming wave was also measured at the observation points on the lower and top boundaries of the computational domain Ω_{FEM}. Thus, we have twice more information at the observation points then in the previous test, and thus, we expect to get more quantitative reconstruction of the photonic crystal.

In Fig. 12-13 we present comparison of the computed L_2-norms of $||E - E_{obs}||_{L_2}$ depending on the relative noise σ on different adaptively refined meshes while the norms decrease. Relative noise σ in data is computed using expression (10.2). From these results we conclude that the reconstruction is stable even with adding 10% noise to the data on two, three and four times refined meshes.

In Fig. 14 we show a comparison of the computed L_2-norms of $||E-E_{obs}||_{L_2}$ depending on the different regularization parameters γ. We see that the smallest value of the difference $||E - E_{obs}||_{L_2}$ we obtain with regularization parameter $\gamma = 0.01$ while choosing $\gamma = 0.1$ is again too large and involve too much regularization. The computational tests show that the best results are obtained on the finest mesh, where $||E-E_{obs}||$ is reduced approximately by a factor seven between first and last optimization iterations, see Fig. 15-b). Fig. 7-i)-l) shows the corresponding to Fig. 15-b) reconstructed parameter field $\epsilon(x)$ at the final optimization iteration indicating domains with a given parameter value.

11 Conclusions and Remarks

We have devised an explicit, adaptive hybrid FEM/FDM method which can be applied to the reconstruction of the structure of the two-dimensional photonic crystal. The method is hybrid in the sense that different numerical methods, finite elements and finite differences, are used in different parts of the computational domain. The adaptivity is based on a posteriori error estimates for the associated Lagrangian in the form of space-time integrals of residuals multiplied by dual weights. We illustrated their usefulness for adaptive error control on an inverse scattering problem for recovering electric permittivity from boundary measured data.

References

[1] L. Sanchis A.Håkansson, J.S. Dehesa. Inverse design of photonic crystal devices. *IEEE Journal on selected areas in communications*, 23 (7):1365 – 1371, 2005.

[2] R. Becker. Adaptive finite elements for optimal control problems. *Habilitationsschrift*, 2001.

[3] R. Becker and R. Rannacher. An optimal control approach to a posteriori error estimation in finite element methods. *Acta Numerica, Cambridge University Press*, pages 1–225, 2001.

[4] L. Beilina. Adaptive FEM method for an inverse scattering problem. *J. Inverse Problems and Information Technologies*, 1, 2-nd issue, 2003.

[5] L. Beilina. *Adaptive finite element/difference methods for time-dependent inverse scattering problems*. PhD thesis, Department of Computational Mathematics, Chalmers University of Technology, 2003.

[6] L. Beilina and C. Clason. An adaptive hybrid fem/fdm method for an inverse scattering problem in scanning acoustic microscopy. *J. SIAM Sci.Comp.*, 28(1), 2006.

[7] L. Beilina and C. Johnson. A Hybrid FEM/FDM method for an Inverse Scattering Problem. In *Numerical Mathematics and Advanced Applications - ENUMATH 2001*. Springer-Verlag, 2001.

[8] L. Beilina and C. Johnson. A posteriori error estimation in computational inverse scattering. *J. Mathematical models and methods in applied sciences*, 15(1):23–37, 2005.

[9] L. Beilina, K. Samuelsson, and K. Åhlander. Efficiency of a hybrid method for the wave equation. In *International Conference on Finite Element Methods*, Gakuto International Series Mathematical Sciences and Applications. Gakkotosho CO.,LTD, 2001.

[10] Eli Yablonovitch Chiu Yen Kao, Stanley Osher. Maximizing band gaps in two-dimensional photonic crystals by using level set methods. *Applied Physics B: Lasers and Optics*, 81:235 – 244, 2005.

[11] G. C. Cohen. *Higher Order numerical methods for transient wave equations*. Springer Verlag, 2002.

[12] D.C.Dobson. An efficient method for band structure calculations in 2d photonic crystals. *JCP*, 149:363 – 376, 1999.

[13] B. Engquist and A. Majda. Absorbing boundary conditions for the numerical simulation of waves. *Math. Comp.*, 31:629–651, 1977.

[14] K. Eriksson, D. Estep, and C. Johnson. *Computational Differential Equations*. Studentlitteratur, Lund, 1996.

[15] Joshua N. Winn John D. Joannopoulos, Robert D. Meade. *Photonic Crystals: Molding the Flow of Light*. Princeton Unviersity Press, 1995.

[16] P. Joly. *Variational methods for time-dependent wave propagation problems.* Lecture Notes in Computational Science and Engineering, Springer, 2003.

[17] E. Yablonovitch M. Burger, S. Osher. Inverse problem techniques for the design of photonic crystals. *IEICE Transactions on Electronics*, 87:258 – 265, 2004.

[18] J. Nocedal. Updating quasi-newton matrices with limited storage. *J. Mathematical of Comp.*, 35, N.151:773–782, 1991.

[19] O. Pironneau. *Optimal shape design for elliptic systems.* Springer Verlag, Berlin, 1984.

[20] P.Kuchment. The mathematics of photonic crystals. *SIAM Mathematical Modeling in Optical Science*, pages 207 – 272, 2001.

[21] E. Yablonovitch. Photonic crystals: Semiconductors of light. *Scientific American*, 285, N. 6:47–55, 2001.